Numerical implementation of a CTO-based implicit approach for the BEM solution of usual and sensitivity problems in elasto-plasticity

Harrison Poon, Subrata Mukherjee, Marc Bonnet

Numerical implementation of a CTO-based implicit approach for the BEM solution of usual and sensitivity problems in elasto-plasticity

Harrison Poon and Subrata Mukherjee
Dept. of Theoretical and Applied Mechanics, Cornell University
Ithaca, NY 14853, USA

Marc Bonnet
Laboratoire de Mécanique des Solides, CNRS URA 317
centre commun Polytechnique, Mines, Ponts et Chausées
Ecole Polytechnique, Palaiseau, France

Engineering Analysis with Boundary Elements, **22**:257–269 (1998)

ABSTRACT

Boundary element method (BEM) formulations for usual and sensitivity problems in small strain elastoplasticity, using the concept of the consistent tangent operator (CTO), have been recently proposed by Bonnet and Mukherjee. 'Usual' problems here refer to analysis of nonlinear problems in structural and solid continua, for which Simo and Taylor first proposed the use of the CTO within the context of the finite element method (FEM). It was shown by Bonnet and Mukherjee that the sensitivity of the strain increment, associated with an infinitesimal variation of some design parameter, solves a linear problem which is governed by the (converged value of the) same global CTO as the one that appears in the usual problem.

This paper presents a general numerical implementation of the above formulations. Numerical results for both the usual and sensitivity problems are presented for a two-dimensional (plane strain) example. Sensitivities are calculated with respect to a material parameter that characterizes isotropic strain hardening. The crucial role of the CTO, in providing accurate numerical results for the mechanical variables as well as their sensitivities, is examined in this paper.

1 INTRODUCTION

This paper is concerned with an implicit Boundary Element Method (BEM) formulation, and numerical implementation, for usual and sensitivity analysis of small strain elasto-plastic problems. The CTO plays a pivotal role in the present development. It enhances the mathematical elegance of the implicit approach by furnishing the exact "derivative" for

the Newton Rhapson procedure, thereby speeding up the rate of convergence. (Quadratic convergence is achieved with the CTO.) But, more importantly, it serves as a crucial link in making possible the accurate computation of design sensitivities, a long-standing challenge faced by many BEM researchers. The basic ideas, together with numerical results for a 1-D implementation, have been presented before [1]. A more general 2-D implementation, with numerical results for an illustrative problem, are presented here.

Sensitivity analysis of nonlinear (material and/or geometrical) problems in solid mechanics is an active research area at present. In this context, design sensitivity coefficients (DSCs) are rates of change of response quantities, such as stresses or displacements in a loaded body, with respect to design variables. These design variables could be shape parameters, sizing parameters, boundary conditions, material parameters etc. DSCs are useful in diverse applications, a very important one being optimal design using gradient based optimization algorithms. Such analyses can be applied, for example, to optimal design of certain manufacturing processes.

Currently, the direct differentiation approach (DDA) or the adjoint structure approach (ADA) are popular for accurate sensitivity analysis. Either of these can be applied in conjunction with general purpose numerical methods such as the finite element method (FEM) or the BEM. The FEM has been used for sensitivity analysis of nonlinear problems by, among others, Arora and his co-workers [2, 3, 4], Choi and his co-workers [5, 6], Haber and his co-workers [7, 8], Kleiber and his co-workers [9, 10, 11], Michaleris *et al.* [12] and Badrinarayanan and Zabaras [13]. Haber, Kleiber and their associates were the first to point out that the consistent (or algorithmic) tangent operator (CTO) (as opposed to the continuum tangent operator) plays a key role in nonlinear sensitivity analysis. The CTO was originally proposed by Simo and Taylor [14] for FEM analysis of (usual) nonlinear problems. The sensitivity problem is always linear (even if the usual problem is not) and the global or system matrix related to the CTO is precisely the stiffness matrix for these problems. Use of the CTO, as pointed out by Kleiber, Haber and their associates, provides very accurate numerical results for sensitivities, while other approaches (e.g. using the continuum tangent) might lead to significant errors. These researchers present numerical results for materially nonlinear problems. Michaleris *et al.* [12], in a recent paper, present sensitivity formulations for general transient nonlinear coupled problems, together with an accurate numerical procedure for the calculation of the CTO. Badrinarayanan and Zabaras [13] present a consistent scheme for sensitivity analysis of nonlinear (both material and geometric) problems in solid mechanics. This paper presents very accurate numerical results for sensitivities at the end of a large deformation (extrusion) process.

All the researchers cited above have employed the FEM in order to obtain their nu-

merical results. Mukherjee and his co-workers have been active in solving nonlinear (both material and geometric) sensitivity problems by the BEM. Examples of the work of this group, using the explicit BEM, are Zhang *et al.* [15, 16] and Leu and Mukherjee [17] (see also the book: Chandra and Mukherjee [18]). Wei *et al.* [19] have used sensitivities to carry out shape optimal design of an elasto-plastic problem.

Most of the publications on BEM analysis of (usual) nonlinear problems in solid mechanics report on the use of the explicit approach for time integration of the appropriate rate equations. Banerjee and his co-workers [20] have presented variable stiffness formulations for such problems. Implicit BEM formulations have been presented by Jin *et al.* [21] and Telles and Carrer [22, 23]. Mukherjee and his co-workers have been interested in implicit sensitivity calculations, using the BEM, during the last few years. Leu and Mukherjee [24, 25] have presented implicit objective integration schemes for recovery of stress sensitivities at a material point. This work addresses large strain viscoplastic problems but only considers integration of the algorithmic constitutive model (analogous to the radial return algorithm) at a material point. They have coupled this analysis with the BEM (Leu and Mukherjee [26]) to solve general boundary value problems. The CTO, however, has not been employed in the work by Leu and Mukherjee cited above. It is observed (Leu and Mukherjee [26]) that stress sensitivities at some material points, at the end of a large deformation process, can exhibit significant numerical errors.

The remedy appears to be an implicit BEM formulation that employs the consistent tangent operator. Within the context of the BEM, Bonnet and Mukherjee [1] have presented, for the first time, an implicit scheme that explicitly utilizes the CTO, together with excellent preliminary numerical results based on a 1-D implementation. A spherical cavity in an infinite domain is loaded with uniform internal pressure. Casting the governing integral equations in the interesting (radial) direction allows for a 1-D BEM solution with 0-D boundary points and 1-D internal cells. Results demonstrate the extreme efficiency and robustness of the approach — accurate answers are obtained with tremendous step sizes (up to 6 times the first yielding pressure) and few iterations. The final converged quantities exhibit apparent insensitivity to the load step size. This issue is discussed further later in the present paper.

The present paper continues the line of work described above, implementing the new implicit scheme in a completely general two dimensional setting. The key equations from Bonnet and Mukherjee [1] are first recapitulated for the sake of completeness. Numerical results for an illustrative 2-D example are presented in section 5 of this paper.

2 IMPLICIT BEM FORMULATION WITH CTO

2.1 BEM equations

The starting point is the boundary integral equation (BIE) (without body forces)

$$\int_{\partial\Omega}[u_i(\boldsymbol{z})-u_i(\boldsymbol{x})]P_i^k(\boldsymbol{x},\boldsymbol{z})dS_z-\int_{\partial\Omega}p_i(\boldsymbol{z})U_i^k(\boldsymbol{x},\boldsymbol{z})dS_z=\int_{\Omega}U_{i,j}^k(\boldsymbol{x},\boldsymbol{z})C_{ijab}\varepsilon_{ab}^p(\boldsymbol{z})dV_z \quad (1)$$

where $\boldsymbol{x}$ is any fixed source point on the boundary $\partial\Omega$, U_i^k, P_i^k denote the components of the Kelvin kernels for displacement and traction, $\boldsymbol{p}=\boldsymbol{\sigma}\cdot\boldsymbol{n}$ is the traction vector. The variable field point is denoted by $\boldsymbol{z}$ and $_{,j}\equiv\partial/\partial\boldsymbol{z}_j$. The tensor C_{ijkl} is the usual Hookean elasticity tensor, which, for isotropic elasticity has the form

$$C_{ijkl}=\frac{2G\nu}{1-2\nu}\delta_{ij}\delta_{kl}+G(\delta_{ik}\delta_{jl}+\delta_{il}\delta_{jk})$$

where G is the shear modulus and ν the Poisson's ratio.

The matrix equation implied by the above BIE reads:

$$[\boldsymbol{H}]\{\boldsymbol{u}\}-[\boldsymbol{G}]\{\boldsymbol{p}\}=[\boldsymbol{Q}]\{\boldsymbol{C}:\boldsymbol{\varepsilon}^p\}$$

which, after the standard operation of "collecting" boundary unknowns, becomes ($\boldsymbol{y}$ being the vector of boundary unknowns):

$$[\boldsymbol{A}]\{\boldsymbol{y}\}=\{\boldsymbol{f}\}+[\boldsymbol{Q}]\{\boldsymbol{C}:\boldsymbol{\varepsilon}^p\} \quad (2)$$

Next, the displacement at an internal point is given by:

$$\begin{aligned}u_k(\boldsymbol{x})=&\int_{\partial\Omega}\left\{p_i(\boldsymbol{z})U_i^k(\boldsymbol{x},\boldsymbol{z})-u_i(\boldsymbol{z})P_i^k(\boldsymbol{x},\boldsymbol{z})\right\}dS_z\\&+\int_{\Omega}U_{i,j}^k(\boldsymbol{x},\boldsymbol{z})C_{ijab}\varepsilon_{ab}^p(\boldsymbol{z})dV_z\end{aligned} \quad (3)$$

which, after differentiation w.r.t. x_ℓ and regularization, yields:

$$\begin{aligned}u_{k,\ell}(\boldsymbol{x})=&\int_{\partial\Omega}u_i(\boldsymbol{z})D_{i\ell}^k(\boldsymbol{x},\boldsymbol{z})dS_z-\int_{\partial\Omega}p_i(\boldsymbol{z})U_{i,\ell}^k(\boldsymbol{x},\boldsymbol{z})dS_z\\&-C_{ijab}\varepsilon_{ij}^p(\boldsymbol{x})\int_{\partial\Omega}n_\ell(\boldsymbol{z})U_{a,b}^k(\boldsymbol{x},\boldsymbol{z})dS_z\\&-\int_{\Omega}U_{i,j\ell}^k(\boldsymbol{x},\boldsymbol{z})C_{ijab}[\varepsilon_{ab}^p(\boldsymbol{z})-\varepsilon_{ab}^p(\boldsymbol{x})]dV_z\end{aligned} \quad (4)$$

using the notation $D_{i\ell}^k=P_{i,\ell}^k$. The well-known kinematic relationship between strain components and displacement gradients allows us to write:

$$\begin{aligned}\{\boldsymbol{\varepsilon}\}&=[\boldsymbol{G}']\{\boldsymbol{p}\}-[\boldsymbol{H}']\{\boldsymbol{u}\}+[\boldsymbol{Q}']\{\boldsymbol{C}:\boldsymbol{\varepsilon}^p\}\\&=-[\boldsymbol{A}']\{\boldsymbol{y}\}+\{\boldsymbol{f}'\}+[\boldsymbol{Q}']\{\boldsymbol{C}:\boldsymbol{\varepsilon}^p\}\end{aligned} \quad (5)$$

At this stage, we point out that certain integrals in (4) become hypersingular when $\boldsymbol{x}$ lies on the boundary. As a result, the boundary strains must be computed carefully. We will return to this important issue later. For now, suffice to say that the strain at a boundary point is still expressable in terms of boundary tractions and displacements and domain plastic strains. In other words, (5) remains valid.

Substituting for $\{\boldsymbol{y}\}$ from (2) into (5) yields:

$$\{\boldsymbol{\varepsilon}\} = \{\boldsymbol{n}\} + [\boldsymbol{S}]\{\boldsymbol{C} : \boldsymbol{\varepsilon}^p\} \tag{6}$$

where

$$\{\boldsymbol{n}\} = \{\boldsymbol{f}'\} - [\boldsymbol{A}'][\boldsymbol{A}]^{-1}\{\boldsymbol{f}\}$$
$$[\boldsymbol{S}] = [\boldsymbol{Q}'] - [\boldsymbol{A}'][\boldsymbol{A}]^{-1}[\boldsymbol{Q}]$$

Note that $\{\boldsymbol{n}\}$ denotes the purely elastic solution, i.e. the one obtained for the same loading but in the absence of plastic strain.

At this point we recall Hooke's law and the additive decomposition of strain:

$$\boldsymbol{\sigma} = \boldsymbol{C} : (\boldsymbol{\varepsilon} - \boldsymbol{\varepsilon}^p) \tag{7}$$

or

$$\{\boldsymbol{C} : \boldsymbol{\varepsilon}^p\} = \{\boldsymbol{C} : \boldsymbol{\varepsilon}\} - \{\boldsymbol{\sigma}\}$$

giving:

$$\{\boldsymbol{\varepsilon}\} = \{\boldsymbol{n}\} + [\boldsymbol{S}](\{\boldsymbol{C} : \boldsymbol{\varepsilon}\} - \{\boldsymbol{\sigma}\})$$

or

$$[\boldsymbol{S}]\{\boldsymbol{\sigma} - \boldsymbol{C}\boldsymbol{\varepsilon}\} - \{\boldsymbol{n}\} + [\boldsymbol{I}]\{\boldsymbol{\varepsilon}\} = \{\boldsymbol{0}\} \tag{8}$$

It is worth mentioning that the foregoing development closely resembles the one presented in Telles and Carrer [22]. The breakthrough ideas which distinguish the present formulation from earlier implicit schemes lie in the intelligent incorporation of the CTO, and the subsequent bonus this confers on the (incrementally linear) sensitivity problem.

The CTO concept is tied to the more fundamental Radial Return Algorithm (RRA). Both are explained in detail in Simo and Taylor [14] and are briefly summarized in the next section.

2.2 RRA and CTO: a summary

The RRA was given in Simo and Taylor [14] in the context of rate-independent plasticity with the Von Mises yield criterion and an associative flow rule. Both isotropic and

kinematic hardening can be accounted for. For simplicity, only isotropic hardening is considered in the present work. (Kinematic hardening is included in Bonnet and Mukherjee [1]).

In computational plasticity, the elastoplastic constitutive law for a finite time step Δt reduces to giving a rule which outputs, $\boldsymbol{\sigma}_{n+1}$ consistent with the yield criterion, for any given strain increment $\Delta\boldsymbol{\varepsilon}_n = \boldsymbol{\varepsilon}_{n+1} - \boldsymbol{\varepsilon}_n$ (input):

$$\boldsymbol{\sigma}_{n+1} = \bar{\boldsymbol{\sigma}}(\boldsymbol{\varepsilon}_n, \boldsymbol{\sigma}_n, \bar{e}^p_n, \Delta\boldsymbol{\varepsilon}_n) \tag{9}$$

Here, the notation $\bar{\boldsymbol{\sigma}}$ symbolically denotes the action of the radial return algorithm (RRA) of Simo and Taylor [14]. $\bar{e}^p$ is the cumulated equivalent plastic strain:

$$\bar{e}^p = \int_0^t \sqrt{\tfrac{2}{3}}\, ||\boldsymbol{d}^p(\tau)||\, d\tau$$

where $\boldsymbol{d}^p$ is the plastic strain rate, with $\mathrm{tr}(\boldsymbol{d}^p) = 0$. Also, the subscript n in $(\boldsymbol{\varepsilon}_n, \ldots)$ refers to time (or pseudo-time) t_n, tr is the trace of the tensor $\boldsymbol{d}^p$ and

$$||\boldsymbol{d}^p(\tau)|| = [\boldsymbol{d}^p : \boldsymbol{d}^p]^{1/2} = +\sqrt{d^p_{ij} d^p_{ij}}$$

The yield condition is

$$f(\boldsymbol{\xi}, \kappa) \equiv ||\boldsymbol{\xi}|| - \sqrt{\tfrac{2}{3}}\kappa(\bar{e}^p) = 0 \tag{10}$$

where $\boldsymbol{\xi} = \boldsymbol{s}$ is the deviatoric stress $\boldsymbol{\sigma} - \frac{1}{3}(\mathrm{tr}\boldsymbol{\sigma})\mathbf{1}$. Here, $\mathbf{1}$ is the second order unit tensor. Also, $\bar{e}^p \to \kappa(\bar{e}^p)$ is the hardening rule.

A trial deviatoric stress is introduced as

$$\boldsymbol{\xi}^T_{n+1} = \boldsymbol{s}_n + 2G\Delta\boldsymbol{e}_n$$

where $\boldsymbol{e} = \boldsymbol{\varepsilon} - \frac{1}{3}(\mathrm{tr}\boldsymbol{\varepsilon})\mathbf{1}$ and G is the shear modulus.

If $f(\boldsymbol{\xi}^T_{n+1}, \kappa_n) \leq 0$, i.e. $\boldsymbol{\xi}^T_{n+1}$ is elastic, one has

$$\bar{\boldsymbol{\sigma}} = K\Delta\boldsymbol{\varepsilon}_n : (\mathbf{1} \otimes \mathbf{1}) + 2G\Delta\boldsymbol{e}_n + \boldsymbol{\sigma}_n \tag{11}$$

(with K the bulk modulus and $\otimes$ denoting the tensor product) i.e. the elastic constitutive equation in incremental form. On the other hand, if $f(\boldsymbol{\xi}^T_{n+1}, \kappa_n) > 0$, $\bar{\boldsymbol{\sigma}}$ is given by the following equations, which constitute the RRA:

$$\bar{\boldsymbol{\sigma}} = K\boldsymbol{\varepsilon}_{n+1} : (\mathbf{1} \otimes \mathbf{1}) + \boldsymbol{s}_{n+1} \tag{12}$$

$$\boldsymbol{s}_{n+1} = \sqrt{\tfrac{2}{3}}\kappa_{n+1}\hat{\boldsymbol{n}} \tag{13}$$

$$\bar{e}^p_{n+1} = \bar{e}^p_n + \sqrt{\tfrac{2}{3}}[\gamma\Delta t]$$

$$\hat{\boldsymbol{n}} = \frac{1}{\left|\left|\boldsymbol{\xi}^T_{n+1}\right|\right|}\boldsymbol{\xi}^T_{n+1}$$

where $[\gamma\Delta t]$ solves the nonlinear consistency equation

$$\left|\left|\boldsymbol{\xi}^T_{n+1}\right|\right| - \sqrt{\tfrac{2}{3}}\kappa(\bar{e}^p_n + \sqrt{\tfrac{2}{3}}[\gamma\Delta t]) - 2G[\gamma\Delta t] = 0 \tag{14}$$

with $\kappa_n = \kappa(\bar{e}^p_n)$.

A pictorial illustration of the RRA is given in Figure 1, where only the deviatoric components are shown and the actions take place on the π-plane.

The consistent tangent operator (CTO) is the fourth-order tensor $\boldsymbol{C}_{n+1} = \partial\bar{\boldsymbol{\sigma}}/\partial\Delta\boldsymbol{\varepsilon}_n$. It was invented in the finite element context whereby Newton's method is employed to solve the nonlinear virtual work equation. The precise expression for the CTO depends on the particular algorithm $\Delta\boldsymbol{\varepsilon}_n \to \boldsymbol{\sigma}_{n+1}$ chosen. For the RRA presented here, it takes the form:

$$\boldsymbol{C}_{n+1} = K\mathbf{1}\otimes\mathbf{1} + 2G\beta(\boldsymbol{I} - \frac{1}{3}\mathbf{1}\otimes\mathbf{1}) - 2G(\beta-\delta)\hat{\boldsymbol{n}}\otimes\hat{\boldsymbol{n}} \tag{15}$$

where β and δ will be defined in section 3 on sensitivity analysis.

It is important to note that when $\bar{\boldsymbol{\sigma}}(\boldsymbol{\varepsilon}_n, \boldsymbol{\sigma}_n, \bar{e}^p_n, \Delta\boldsymbol{\varepsilon}_n)$ is elastic one has

$$\boldsymbol{C}_{n+1} = \boldsymbol{C} \tag{16}$$

where $\boldsymbol{C}$ is the fourth-order tensor of elastic coefficients that has been defined earlier in section 2.

2.3 Crucial role of the CTO in the present formulation

Bearing in mind the path dependence of plastic deformation, the incremental form of eqn (8) is written:

$$[\boldsymbol{S}]\{\Delta\boldsymbol{\sigma}_n - \boldsymbol{C}\Delta\boldsymbol{\varepsilon}_n\} - \{\Delta\boldsymbol{n}_n\} + [\boldsymbol{I}]\{\Delta\boldsymbol{\varepsilon}_n\} = \{\mathbf{0}\} \tag{17}$$

using the notation $\Delta()_n = ()_{n+1} - ()_n$.

Equation (17) enforces the equilibrium constraint as well as the elastic constitutive law, thanks to Somigliana's identity which underlies Boundary Integral Equation (BIE) formulations.

Meanwhile, the radial return algorithm relates $\bar{\boldsymbol{\sigma}} = \boldsymbol{\sigma}_{n+1} = \boldsymbol{\sigma}_n + \Delta\boldsymbol{\sigma}_n$ to $\Delta\boldsymbol{\varepsilon}_n$. Combining the constitutive and equilibrium equations in the form

$$\{\boldsymbol{\sigma}_n\} + \{\Delta\boldsymbol{\sigma}_n\} = \{\bar{\boldsymbol{\sigma}}\}$$

(where $\Delta\boldsymbol{\sigma}_n(\Delta\boldsymbol{\varepsilon}_n, \cdot\cdot, \cdot\cdot)$ comes from the BEM equation while $\bar{\boldsymbol{\sigma}}(\Delta\boldsymbol{\varepsilon}_n, \cdot\cdot, \cdot\cdot)$ comes from the RRA), we obtain a nonlinear equation for $\Delta\boldsymbol{\varepsilon}_n$ of the form:

$$\{G(\Delta\boldsymbol{\varepsilon}_n)\} \equiv [\boldsymbol{S}]\{\bar{\boldsymbol{\sigma}}(\boldsymbol{\varepsilon}_n, \boldsymbol{\sigma}_n, \bar{e}^p_n, \Delta\boldsymbol{\varepsilon}_n) - \boldsymbol{\sigma}_n - \boldsymbol{C}\Delta\boldsymbol{\varepsilon}_n\} - \{\Delta\boldsymbol{n}_n\} + [\boldsymbol{I}]\{\Delta\boldsymbol{\varepsilon}_n\} = \{\mathbf{0}\} \tag{18}$$

The consistent tangent operator $\boldsymbol{C}_{n+1}$ appears upon application of Newton's method. The additive correction $\delta\boldsymbol{\varepsilon}_n^i = \Delta\boldsymbol{\varepsilon}_n^{i+1} - \Delta\boldsymbol{\varepsilon}_n^i$ to $\Delta\boldsymbol{\varepsilon}_n^i$ solves the equation

$$([\boldsymbol{S}][\boldsymbol{C} - \boldsymbol{C}_{n+1}^i] - [\boldsymbol{I}])\{\delta\boldsymbol{\varepsilon}_n^i\} = \{G(\Delta\boldsymbol{\varepsilon}_n^i)\} \tag{19}$$

The quantity $([\boldsymbol{S}][\boldsymbol{C} - \boldsymbol{C}_{n+1}^i] - [\boldsymbol{I}]) = ([\boldsymbol{D}_{n+1}^i] - [\boldsymbol{I}])$ is hereafter called the global CTO (see Kleiber *et al.* [10] for the FEM version). Once the nonlinear equation (18) is solved for $\Delta\boldsymbol{\varepsilon}_n$, all the variables at time t_{n+1} are readily computed. It is interesting to note that the Newton step (19) involves the difference $[\boldsymbol{C} - \boldsymbol{C}_{n+1}^i]$ between the elastic constitutive law and the local CTO, rather than the local CTO itself; this is entirely consistent with the fact that eqn (17) accounts for equilibrium as well as the elastic constitutive law.

Observe that at those material points where the incremental deformation is purely elastic (i.e. trial stress lies within the yield surface), the local CTO coincides with $\boldsymbol{C}$. The implication is that the quasi-diagonal matrix $[\boldsymbol{C} - \boldsymbol{C}_{n+1}^i]$ can have zero blocks on the diagonal, leading to corresponding zero block columns in the matrix $[\boldsymbol{D}_{n+1}^i]$. Hence, the Newton step (19) admits the following block decomposition:

$$([\boldsymbol{D}_{n+1}^i] - [\boldsymbol{I}])_{PP}\{\delta\boldsymbol{\varepsilon}_n^i\}_P = \{G(\Delta\boldsymbol{\varepsilon}_n^i)\}_P \tag{20}$$

$$\{\delta\boldsymbol{\varepsilon}_n^i\}_E = ([\boldsymbol{D}_{n+1}^i])_{EP}\{\delta\boldsymbol{\varepsilon}_n^i\}_P - \{G(\Delta\boldsymbol{\varepsilon}_n^i)\}_E \tag{21}$$

where the subscripts E, P indicate partitionings based on currently elastic (E) or plastic (P) nodes. Also, use has been made of the conglomeration of zero block columns:

$$[\boldsymbol{D}_{n+1}^i]_{PE} = [\boldsymbol{D}_{n+1}^i]_{EE} = [\boldsymbol{0}]$$

In effect, (20) says that the size of the linear system ties in with the size of the plastically deforming zone, representing significant savings in computer time.

3 SENSITIVITY ANALYSIS

Now we are interested in computing the sensitivities of the mechanical variables associated with an infinitesimal perturbation of some design parameter b of an (as yet) unspecified nature. It should be mentioned here that such sensitivities are expected to suffer jump discontinuities at certain locations, e.g. on the transition interface between the current elastic and plastic zones. Usually, however, this is not a major problem in practical optimization applications. We disregard this issue in the present work and treat sensitivities of mechanical variables as continuous. The reader is referred to Lee and Arora [27] and Bonnet and Mukherjee [1] for further discussion of this issue.

Since sensitivity in the present context means a comparison of two history-dependent mechanical processes, the sensitivity computation must also proceed in an incremental way, resulting in an accumulation of sensitivity increments, each of which is a solution to a linear problem. The adjoint structure approach (ASA), very powerful for steady-state situations, leads to regressive computations when applied to evolution problems. Applied to nonlinear, history-dependent problems, the ASA would require the storage of the whole mechanical history and of the converged tangent operators for all time steps, thus becoming rather impractical. An excellent reference for this area of research is a recent paper by Michaleris *et al.* [12]. In contrast, the direct differentiation approach (DDA) fits perfectly into the progressive time-stepping computational scheme. The DDA is thus preferable for nonlinear evolution problems; it is used in the present work.

It should be mentioned at the outset that the precise details as well as the algebraic complexity of the derivation (of sensitivity equations) depend on the specific choice of the design parameter b. Geometric design parameters, for instance, result in much more tedious algebra than material parameters do. In order to illustrate the process of sensitivity derivation without excessive algebra, we choose a (material) parameter that characterizes (isotropic) strain hardening. More specifically, let

$$\kappa = k_0 + k_1(\bar{e}^p)^m = \kappa(\bar{e}^p, b)$$

where b designates the parameter to be varied and can be any one of k_0, k_1, or m.

Recall the incremental form of the usual problem (eqn 18):

$$[\boldsymbol{S}]\,\{\bar{\boldsymbol{\sigma}}(\boldsymbol{\varepsilon}_n, \boldsymbol{\sigma}_n, \bar{e}^p_n, \Delta\boldsymbol{\varepsilon}_n) - \boldsymbol{\sigma}_n - \boldsymbol{C}\Delta\boldsymbol{\varepsilon}_n\} - \{\Delta\boldsymbol{n}_n\} + [\boldsymbol{I}]\{\Delta\boldsymbol{\varepsilon}_n\} = \{\boldsymbol{0}\}$$

Differentiating w.r.t. b yields: (a $\star$ above a variable denotes a derivative with respect to b)

$$[\boldsymbol{S}]\,\{\overset{\star}{\bar{\boldsymbol{\sigma}}} - \overset{\star}{\boldsymbol{\sigma}}_n - \boldsymbol{C}\overset{\star}{\Delta\boldsymbol{\varepsilon}}_n\} + [\boldsymbol{I}]\{\overset{\star}{\Delta\boldsymbol{\varepsilon}}_n\} + \left[\overset{\star}{\boldsymbol{S}}\right]\{\bar{\boldsymbol{\sigma}} - \boldsymbol{\sigma}_n - \boldsymbol{C}\Delta\boldsymbol{\varepsilon}_n\} - \{\Delta\overset{\star}{\boldsymbol{n}}_n\} = \{\boldsymbol{0}\}$$

where use has been made of the fact that $\boldsymbol{C}$ is independent of b.

The present choice of b implies that both $\{\Delta\overset{\star}{\boldsymbol{n}}_n\}$ (purely elastic strain) and $\left[\overset{\star}{\boldsymbol{S}}\right]$ (which encapsulates, among other things, geometrical information) vanish. We are left with:

$$[\boldsymbol{S}]\,\{\overset{\star}{\bar{\boldsymbol{\sigma}}} - \overset{\star}{\boldsymbol{\sigma}}_n - \boldsymbol{C}\overset{\star}{\Delta\boldsymbol{\varepsilon}}_n\} + [\boldsymbol{I}]\{\overset{\star}{\Delta\boldsymbol{\varepsilon}}_n\} = \{\boldsymbol{0}\} \tag{22}$$

Next, it is necessary to work with the equations governing the RRA. Recall the consistency eqn (14) :

$$\left|\left|\boldsymbol{\xi}^T_{n+1}\right|\right| - \sqrt{\tfrac{2}{3}}\kappa(\bar{e}^p_n + \sqrt{\tfrac{2}{3}}[\gamma\Delta t]) - 2G[\gamma\Delta t] = 0$$

Using the notations:

$$\kappa' = \frac{\partial \kappa}{\partial \bar{e}^p}; \qquad \dot{\kappa} = \frac{\partial \kappa}{\partial b}$$

and the following algebraic manipulations:

$$\begin{aligned} \left|\left|\boldsymbol{\xi}^T_{n+1}\right|\right|^\star &= \hat{\boldsymbol{n}} : \overset{\star}{\boldsymbol{\xi}}{}^T_{n+1} \\ &= \hat{\boldsymbol{n}} : (\overset{\star}{\boldsymbol{\sigma}}_n + 2G\overset{\star}{\Delta}\boldsymbol{\varepsilon}_n) \\ \overset{\star}{\kappa}_{n+1} &= \kappa'_{n+1}\overset{\star}{\bar{e}^p}_{n+1} + \dot{\kappa}_{n+1}\overset{\star}{b} \\ &= \kappa'_{n+1}[\overset{\star}{\bar{e}^p}_n + \sqrt{\tfrac{2}{3}}[\overset{\star}{\gamma}\,\Delta t]] + \dot{\kappa}_{n+1} \end{aligned} \tag{23}$$

we arrive at the differentiated consistency eqn:

$$\hat{\boldsymbol{n}} : (\overset{\star}{\boldsymbol{\sigma}}_n + 2G\overset{\star}{\Delta}\boldsymbol{\varepsilon}_n) - \sqrt{\tfrac{2}{3}}\left\{\kappa'_{n+1}[\overset{\star}{\bar{e}^p}_n + \sqrt{\tfrac{2}{3}}[\overset{\star}{\gamma}\,\Delta t]] + \dot{\kappa}_{n+1}\right\} = 2G[\overset{\star}{\gamma}\,\Delta t]$$

Upon grouping terms, one gets the following scalar linear equation for $[\overset{\star}{\gamma}\,\Delta t]$:

$$(\tfrac{2}{3}\kappa'_{n+1} + 2G)[\overset{\star}{\gamma}\,\Delta t] = \hat{\boldsymbol{n}} : (\overset{\star}{\boldsymbol{\sigma}}_n + 2G\overset{\star}{\Delta}\boldsymbol{\varepsilon}_n) - \sqrt{\tfrac{2}{3}}(\kappa'_{n+1}\overset{\star}{\bar{e}^p}_n + \dot{\kappa}_{n+1})$$

which readily gives

$$2G[\overset{\star}{\gamma}\,\Delta t] = (1-\delta)\hat{\boldsymbol{n}} : (\overset{\star}{\boldsymbol{\sigma}}_n + 2G\overset{\star}{\Delta}\boldsymbol{\varepsilon}_n) - (1-\delta)\left(\theta\left|\left|\boldsymbol{\xi}^T_{n+1}\right|\right|\overset{\star}{\bar{e}^p}_n + \sqrt{\tfrac{2}{3}}\dot{\kappa}_{n+1}\right) \tag{24}$$

where the abbreviated notations

$$\theta = \frac{\sqrt{\frac{2}{3}}\kappa'_{n+1}}{\left|\left|\boldsymbol{\xi}^T_{n+1}\right|\right|}$$
$$\delta = \frac{\kappa'_{n+1}}{\kappa'_{n+1} + 3G}$$

have been used.

Next consider the deviatoric stress:

$$\boldsymbol{s}_{n+1} = \sqrt{\tfrac{2}{3}}\kappa_{n+1}\hat{\boldsymbol{n}} \tag{13}$$

which, upon differentiation, gives:

$$\overset{\star}{\boldsymbol{s}}_{n+1} = \sqrt{\tfrac{2}{3}}\overset{\star}{\kappa}_{n+1}\hat{\boldsymbol{n}} + \sqrt{\tfrac{2}{3}}\kappa_{n+1}\overset{\star}{\hat{\boldsymbol{n}}} \tag{25}$$

Applying the product rule to the definition $\hat{\boldsymbol{n}} = \boldsymbol{\xi}_{n+1}^T / \left|\left|\boldsymbol{\xi}_{n+1}^T\right|\right|$, and making use of (23), one readily sees that:

$$\overset{\star}{\hat{\boldsymbol{n}}} = \frac{1}{\left|\left|\boldsymbol{\xi}_{n+1}^T\right|\right|}(\boldsymbol{I} - \frac{1}{3}\mathbf{1}\otimes\mathbf{1} - \hat{\boldsymbol{n}}\otimes\hat{\boldsymbol{n}}) : (\overset{\star}{\boldsymbol{\sigma}}_n + 2G\overset{\star}{\Delta\boldsymbol{\varepsilon}}_n) \tag{26}$$

Using equations $(23)_2$, $(23)_4$, (24) and (26) in equation (25)) and grouping terms appropriately, one gets

$$\begin{aligned}\overset{\star}{\boldsymbol{s}}_{n+1} = {} & [\beta(\boldsymbol{I} - \frac{1}{3}\mathbf{1}\otimes\mathbf{1}) - (\beta-\delta)\hat{\boldsymbol{n}}\otimes\hat{\boldsymbol{n}}] : (\overset{\star}{\boldsymbol{\sigma}}_n + 2G\overset{\star}{\Delta\boldsymbol{\varepsilon}}_n) \\ & + \theta(1-\delta)\boldsymbol{\xi}_{n+1}^T\overset{\star}{\bar{e}^p}_n + (1-\delta)\sqrt{\tfrac{2}{3}}\dot{\kappa}_{n+1}\hat{\boldsymbol{n}}\end{aligned} \tag{27}$$

where the new parameter β (as in Simo and Taylor [14]) is:

$$\beta = \sqrt{\frac{2}{3}}\frac{\kappa_{n+1}}{\left|\left|\boldsymbol{\xi}_{n+1}^T\right|\right|}$$

Note that the parameters β and δ appeared before in the CTO expression in equation (15).

Combining the above equation with the sensitivity version of (12), we obtain the sensitivity of the radial return algorithm as

$$\begin{aligned}\overset{\star}{\boldsymbol{\sigma}} = {} & \left[\beta(\boldsymbol{I} - \frac{1}{3}\mathbf{1}\otimes\mathbf{1}) - (\beta-\delta)\hat{\boldsymbol{n}}\otimes\hat{\boldsymbol{n}}\right] : \overset{\star}{\boldsymbol{\sigma}}_n + K\mathbf{1}\otimes\mathbf{1} : \overset{\star}{\boldsymbol{\varepsilon}}_n \\ & + \left\{K\mathbf{1}\otimes\mathbf{1} + 2G\beta(\boldsymbol{I} - \frac{1}{3}\mathbf{1}\otimes\mathbf{1}) - 2G(\beta-\delta)\hat{\boldsymbol{n}}\otimes\hat{\boldsymbol{n}}\right\} : \overset{\star}{\Delta\boldsymbol{\varepsilon}}_n \\ & + \theta(1-\delta)\boldsymbol{\xi}_{n+1}^T\overset{\star}{\bar{e}^p}_n + (1-\delta)\sqrt{\tfrac{2}{3}}\dot{\kappa}_{n+1}\hat{\boldsymbol{n}}\end{aligned} \tag{28}$$

It is very important to note that the factor multiplying $\overset{\star}{\Delta\boldsymbol{\varepsilon}}_n$ in (28) is equal to the converged value of the consistent tangent operator $\boldsymbol{C}_{n+1}$ as given in Simo and Taylor [14] (see equation (15)).

Finally, substitution of (28) into (22) gives a *linear* equation for $\{\overset{\star}{\Delta\boldsymbol{\varepsilon}}_n\}$ of the form

$$([\boldsymbol{S}][\boldsymbol{C} - \boldsymbol{C}_{n+1}] - [\boldsymbol{I}])\{\overset{\star}{\Delta\boldsymbol{\varepsilon}}_n\} = \{\boldsymbol{F}\}$$

where the load vector $\{\boldsymbol{F}\}$ is given by:

$$\begin{aligned}\{\boldsymbol{F}\} = [\boldsymbol{S}]\Big\{ & [\beta(\boldsymbol{I} - \frac{1}{3}\mathbf{1}\otimes\mathbf{1}) - (\beta-\delta)\hat{\boldsymbol{n}}\otimes\hat{\boldsymbol{n}}] : \overset{\star}{\boldsymbol{\sigma}}_n \\ & - \overset{\star}{\boldsymbol{\sigma}}_n + \theta(1-\delta)\boldsymbol{\xi}_{n+1}^T\overset{\star}{\bar{e}^p}_n + (1-\delta)\sqrt{\tfrac{2}{3}}\dot{\kappa}_{n+1}\hat{\boldsymbol{n}} \\ & + K\mathbf{1}\otimes\mathbf{1} : \overset{\star}{\boldsymbol{\varepsilon}}_n\Big\}\end{aligned}$$

The matrix multiplying $\overset{\star}{\Delta}\boldsymbol{\varepsilon}_n$ is the converged value of the "global (or system) consistent tangent matrix" (see equation (19)). The block decomposition strategy applies here as well:

$$([\boldsymbol{D}^i_{n+1}] - [\boldsymbol{I}])_{PP}\{\overset{\star}{\Delta}\boldsymbol{\varepsilon}_n\}_P = \{\boldsymbol{F}\}_P \tag{29}$$

$$\{\overset{\star}{\Delta}\boldsymbol{\varepsilon}_n\}_E = ([\boldsymbol{D}^i_{n+1}])_{EP}\{\overset{\star}{\Delta}\boldsymbol{\varepsilon}_n\}_P - \{\boldsymbol{F}\}_E \tag{30}$$

4 COMPUTATIONAL ALGORITHM

The following pseudo-code outlines the overall solution procedure, from initial time t_0 to final time t_{N_T}. The initial time t_0 corresponds to the first yield load.

For $0 \le n \le (N_T - 1)$:

1. Compute $\{\Delta n_n\}$ (purely elastic internal strain)
2. Initialize $\{\Delta\boldsymbol{\varepsilon}^0_n\}$ (e.g. to the elastic value)

   Iterative solution of (18):

   (a) $i = 0$

   (b) Compute the residual $\{G(\Delta\boldsymbol{\varepsilon}^i_n)\}$ from (18). (This requires iterative solution of $[\gamma\Delta t]$ from the RRA.)

   (c) Convergence test: if $\{G(\Delta\boldsymbol{\varepsilon}^i_n)\} \le$ EPS, GOTO 3.

   (d) $i := i + 1$

   (e) Compute the local CTOs $\boldsymbol{C}^i_{n+1}$ at all nodes; classify into currently elastic (E) and plastic (P) sets.

   (f) Set up and factor the global CTO $[\boldsymbol{S}(\boldsymbol{C} - \boldsymbol{C}^i_{n+1}) - \boldsymbol{I}]_{PP}$, set up $[\boldsymbol{S}(\boldsymbol{C} - \boldsymbol{C}^i_{n+1}) - \boldsymbol{I}]_{EP}$.

   (g) Solve (20) for $\{\delta\boldsymbol{\varepsilon}^i_n\}_P$ and compute $\{\delta\boldsymbol{\varepsilon}^i_n\}_E$ using (21).

   (h) Update: $\{\Delta\boldsymbol{\varepsilon}^i_n\} := \{\Delta\boldsymbol{\varepsilon}^i_n\} + \{\delta\boldsymbol{\varepsilon}^i_n\}$.

   (i) GOTO (b) (start new iteration).

3. Update: $\{\bar{e}^p\}_{n+1} = \{\bar{e}^p\}_n + \sqrt{\frac{2}{3}}\{[\gamma\Delta t]\}$, $\quad \{\boldsymbol{\sigma}_{n+1}\} = \{\bar{\boldsymbol{\sigma}}(\Delta\boldsymbol{\varepsilon}^i_{n+1})\}$, $\{\boldsymbol{\varepsilon}_{n+1}\} = \{\boldsymbol{\varepsilon}_n\} + \{\Delta\boldsymbol{\varepsilon}_n\}$.
4. Sensitivity problem:

   (a) Set up the right-hand sides $\{\boldsymbol{F}\}_P, \{\boldsymbol{F}\}_E$.

   (b) Solve (29) for $\{\overset{\star}{\Delta}\boldsymbol{\varepsilon}_n\}_P$ and compute $\{\overset{\star}{\Delta}\boldsymbol{\varepsilon}_n\}_E$ using (30).

   (c) Update: $\{\overset{\star}{\boldsymbol{\varepsilon}}_{n+1}\} = \{\overset{\star}{\boldsymbol{\varepsilon}}_n\} + \{\overset{\star}{\Delta}\boldsymbol{\varepsilon}_n\}$, $\{\overset{\star}{\bar{e}^p}_{n+1}\} = \{\overset{\star}{\bar{e}^p}_n\} + \sqrt{\frac{2}{3}}\{[\overset{\star}{\gamma}\,\Delta t]\}$ (using eq. (24)), $\{\overset{\star}{\boldsymbol{\sigma}}_{n+1}\} = \{\overset{\star}{\bar{\boldsymbol{\sigma}}}\}$ (using eq. (28))

Continue

As mentioned in section 2.1, the boundary strains are not computable by a straightforward encoding of eqn (4), due to the hypersingular kernels. Instead, we adopt the popular approach that makes use of tangential derivatives of boundary displacements and pointwise application of Hooke's law (see, e.g. the discussion in Sladek and Sladek [28] for the elastic case). This "boundary shortcut" is found to give satisfactory results in the numerical example presented below. For other problems, however, a hypersingular treatment of (4) may be necessary to insure accurate results. Guiggiani [29] illustrates such an approach for the linearly elastic case.

5 NUMERICAL RESULTS

The results presented here relate to internal pressure loading of an elastoplastic hollow cylinder, in plane strain. Even though the physics of this problem is really one dimensional, a general 2-D implementation of the present implicit formulation is employed here. The objective is to assess the performance of the method in a general, "real world" setting, where analytical integrations, such as in the 1-D problem analyzed in Bonnet and Mukherjee [1], are no longer possible.

Despite the apparent physical simplicity of the problem at hand, closed form solutions, describing the evolution of mechanical variables as the plastic front moves outward, are not available for the von Mises yield function case. † As discussed in Hodge and White [30], the process is governed by a hyperbolic system of three quasi-linear first-order partial differential equations, the solution of which can only be effected numerically. (This was done in the same paper.) Here, we use the commercial finite element code ABAQUS to furnish the reference solution.

The hollow cylinder has inner radius 1 and outer radius 2. The elastic constants are: $G = 1, \quad \nu = 0.3$ where G denotes the shear modulus and ν the Poisson ratio. The material deforms plastically according to the classical J2 theory, with isotropic strain hardening of the form:

$$\kappa = 2G(0.001 + 0.001(\bar{e}^p)^m)$$

where m takes on values of 1 or 0.2 depending on the example. The usual practice of non-dimensionalization (e.g. dividing stresses by the shear modulus, radial distances by the inner radius, etc.) becomes unnecessary with the current choice of material parameters.

† One is more fortunate in the spherically symmetric situation where the coincidence of the Tresca and von Mises criteria simplifies the algebra and allows for an exact solution (see, e.g. Bonnet and Mukherjee [1]).

Quadratic interpolation of nodal quantities is used throughout this work. The BEM implementation uses 3-noded boundary elements and 6-noded, triangular internal cells. The FEM setup (ABAQUS) employs 8-noded quadrilateral elements.

To exploit symmetry, only one quarter of the body is modeled in the BEM implementation, while for the FEM, only one sixteenth is modeled. The reason for using such a small slice in the FEM analysis is that we put an extra fine mesh there, in order to generate sufficiently accurate reference solutions. Sample meshes are shown in Figures 2 and 3.

Since ABAQUS (as of version 5.4) does not have built-in capabilities for sensitivity calculations, the FEM sensitivity results shown here are based on the finite difference approach, using 1% perturbation‡ in the design parameter.

5.1 Example 1

This example traces the loading history of the elastoplastic cylinder under increasing internal pressure loading. Linear hardening is considered here, so that the Mises yield stress takes the form:

$$\kappa = 2G(0.001 + 0.001\bar{e}^p)$$

Elasticity calculations reveal that the pressure at first yield is $p_y \approx 8.7 \times 10^{-4}$, while numerical experiments using ABAQUS show that the pressure at which the entire cylinder has yielded is in the neighborhood $p_c \approx 16 \times 10^{-4}$. We choose to apply a maximum pressure of 14×10^{-4}. With such a loading, a significant amount of plastic flow has occurred, yet the plastic front remains inside the body. The total load is divided into 7 equal increments, the first 4 of which are elastic.

Figure 4 shows the evolution of radial stress profiles, computed using a mesh with 6 r-divisions and 14 θ-divisions (exactly the mesh shown in Figure 2). Figure 5 shows the corresponding profiles for hoop stresses. The agreement between BEM and FEM results is excellent.

A few comments are in order here:

1) The BEM results (shown as crosses) have been averaged in the hoop direction. Without such adjustments, the computed values tend to fluctuate around the reference solution. This issue is discussed in greater detail, and the phenomenon clearly illustrated, in Example

‡ The fact that ABAQUS outputs only 5 significant digits places severe constraints on finite difference sensitivity calculations. Too small a perturbation can result in differences beyond the 5 digits. Too large a perturbation violates the mathematical definition. The value 1% was found by trial and error to be a reasonable compromise.

2. The ABAQUS results, on the other hand, need no special treatment – the very fine mesh already gives rise to smooth, highly accurate results.
2) The same problem has been re-analyzed using just 1 load increment, resulting in a final state that is virtually identical * to the final state from the multi-step analysis. This interesting observation is important in its own right and the issue involved is discussed at length in section 5.4. It is felt that use of the CTO is essential for the Newton method to converge with such a large load step.
3) ABAQUS is also capable of solving the problem with a single increment, thanks to its incorporation of the CTO in the implicit FEM setting (similar to the one described in Simo and Taylor [14]).

5.2 Example 2

This example concerns nonlinear isotropic hardening of the form:

$$\kappa = 2G(0.001 + 0.001(\bar{e}^p)^m)$$

with $m = 0.2$. The internal pressure of 19×10^{-4} is chosen so that a good portion (but not all) of the cylinder has yielded. This time, only one increment is used. (Re-analysis using multiple increments confirms the validity of this choice – see the remarks in section 5.4) The focus here is on the oscillatory behavior exhibited by the BEM results in the absence of averaging.

Figures 6, 7, and 8 show, respectively, the radial stress, hoop stress, and sensitivity of the hoop stress w.r.t. m. The circles, which mark the BEM results without averaging (along a radial edge in the quarter hollow cylinder), follow a visible pattern of small oscillations around the solid line (ABAQUS reference solution). The oscillation is largely reduced upon averaging (see the crosses), implying a higher level of accuracy globally than on the boundary.

The origin of the oscillation appears to be the use of the "boundary shortcut" mentioned in section 4. The shortcut utilizes strictly local information, whereas formula (4) for internal strains makes use of data over the entire boundary and domain. As a matter of fact, Guiggiani [29] reported the same situation in linear elasticity, and proposed an algorithm to accurately evaluate the hypersingular integrals associated with boundary points, resulting in super-accurate results. It is expected that similar hypersingular algorithms, when applied to the present elastoplastic case, will eliminate the boundary oscillations

* the minute difference in computer outputs can be attributed to the accumulation of rounding error in the incrementation process

altogether, and yield even more accurate results globally, without the need for any kind of averaging.

The accuracy of the ABAQUS sensitivity solution in Figure 8 is questionable (see the next section).

5.3 Example 3

In example 2, it is seen (Figure 8) that the agreement between BEM and FEM results is less than perfect when it comes to hoop stress sensitivity. However, the accuracy of the FEM sensitivity results, obtained by finite differencing of a pair of neighboring FEM solutions, is somewhat questionable (see the discussion immediately before Example 1). In order to reliably assess the BEM sensitivity computation, we concoct a simple example where the sensitivity can be obtained exactly.

The hollow cylinder is subjected to equal internal and external pressures $p_o = p_i = 0.01$. The deformation is homogeneous. The hardening law is:

$$\kappa = 2G(0.001 + k_1 \bar{e}^p)$$

and the sensitivity of $\bar{e}^p$ w.r.t. k_1 at $k_1 = 0.001$ is sought. The derivation of the exact solution $\overset{\star}{\bar{e}}{}^p = -5.9080669 \times 10^{-4}$ is shown in the Appendix.

The problem is analyzed with one load step, using a coarser mesh with 4 r-divisions and 9 θ-divisions. Table 1 shows the highly accurate results, with a maximum error of only 0.3% even for the non-averaged numerical results.

5.4 A comment on the effects of load step size

It is interesting to note that, in both the 1-D example presented in Bonnet and Mukherjee [1] and the present result, the final converged quantities exhibit apparent insensitivity to the load step size. In other words, the final answer appears to be the same whether one uses ten increments or applies the entire load in one step. This may seem counter-intuitive, given the path dependent nature of plastic deformation.

To shed some light on this issue, let us focus attention on a single continuum point, where the elastoplastic constitutive law (RRA) is applied. A very important point to realize is that the RRA integrates the plasticity evolution equations only approximately. Consider the situation illustrated in Figure 9 (where strain hardening is absent, to simplify matters). The initial stress state is denoted by point A, while AB represents the total deformation we apply. A single RRA step (ABC) leads to a final stress at point C. However, if we break the applied loading into two parts (AD and $DB = EF$) and perform a sequence of

two RRA steps (ADEFG), we arrive at a different final state at point G. Such sensitivity to load step size is a clear indication of the "inexactness" of the (plasticity) integration algorithm, in much the same way that the influence of step size on accuracy reveals the approximate nature of Runge Kutta as a tool to integrate ODE's.

The discussion so far points to the use of suitably small load steps in order to reasonably capture the evolution of mechanical variables in a plastic process. However, a lucky situation arises when every point in the body undergoes proportional loading (i.e. the loading path is a straight line through the origin). When that is the case, the normal $\hat{\boldsymbol{n}}$ to the yield surface stays constant, and the plasticity integration implied by the RRA turns out to be exact. Consequently, there is no need to subdivide the load. Both the hollow cylinder considered here and the hollow sphere in an infinite medium in Bonnet and Mukherjee [1] fall under this category.

Furthermore, even in cases like Figure 9, the difference may not be perceptible in results plots, especially in small strain plasticity (Figure 9 is a highly exaggerated drawing). To better appreciate the effects of load incrementation, one may go to large deformations. The reader is referred to the paper by Arif and Zabaras [31] for a vivid example. There, a cylindrical billet undergoes 60% upset forging. The (FEM) analysis was repeated with different numbers of load steps. The minimum allowable number of steps (without divergence of Newton's method) was only **two**, demonstrating the great virtue of the CTO. The final deformed meshes, however, were noticeably different.

In view of the foregoing discussion, the authors offer the following advice:
Since plastic flow is inherently path dependent, the load steps must be small enough to reasonably capture the evolution of mechanical variables. The use of a single load step is valid only for certain fortuitous situations, such as when every continuum point undergoes proportional loading. Without a priori information about the loading path shapes at different points of the body, one should not blindly trust the results from a one (or very few) step analysis. Instead, repeating the analysis using more load steps and comparing the results is a recommended course of action.

6 CONCLUSIONS

It has been pointed out by Bonnet and Mukherjee [1], as well as by other authors (e.g. Vidal and Haber [8] and Kleiber [9]), that use of the CTO is crucial for obtaining accurate numerical results for sensitivities of variables governed by nonlinear equations such as in elastoplasticity. The reason is that use of another operator (e.g. the continuum tangent), while destroying quadratic convergence of the associated Newton method, might still lead to slower convergence to the true solution. The sensitivity problem, however, is linear, and

its stiffness matrix is obtained from the converged value of the CTO for that load step. Thus, use of a different operator would very likely lead to significant errors in numerical results for sensitivities.

The above assertion is supported by the numerical results presented in this paper. It is seen from Table 1 that, for example 3 for which an exact value of the sensitivity is available, the maximum numerical error at any point in the cylinder is of the order of 0.3%.

Another major advantage of using the CTO is related to efficiency. In example 2, with nonlinear work hardening, the converged solution of the usual problem is obtained in one load step, even though the chosen internal pressure is such that most of the cylinder undergoes plastic deformation. Use of such a large load step would not be possible without the CTO.

A possible improvement on this work would be the numerical implementation of a hypersingular boundary strain (and stress) representation rather than the currently employed "boundary shortcut". Work along these lines is currently in progress.

ACKNOWLEDGEMENTS

This research was funded by NSF grant number MSS-9301443 to Cornell University. The computing for this research was conducted using the resources of the Cornell Theory Center, which receives major funding from the National Science Foundation and New York State with additional support from the Advanced Research Projects Agency, the National Center for Research Resources at the National Institutes of Health, IBM Corporation and members of the Corporate Research Institute.

REFERENCES

1. Bonnet, M. & Mukherjee, S. Implicit BEM formulations for usual and sensitivity problems in elasto-plasticity using the consistent tangent operator concept. *Int. J. Solids Struct.*, 1996, **33**, 4461–4480.
2. Arora, J.S. & Cardoso, J.B. Variational principle for shape sensitivity analysis. *AIAA Journal*, 1992, **30**, 538–547.
3. Jao, S.Y. & Arora, S.J. Design sensitivity analysis of nonlinear structures using endochronic constitutive model. Part 1: general theory. *Comp. Mech.*, 1992, **10**, 39–57.
4. Jao, S.Y. & Arora, S.J. Design sensitivity analysis of nonlinear structures using endochronic constitutive model. Part 2: discretization and applications. *Comp. Mech.*, 1992, **10**, 59–72.
5. Choi, K.K. & Santos, J.L.T. Variational methods for design sensitivity analysis in nonlinear structural systems; part. I: theory. *Int. J. Num. Meth. in Eng.*, 1987, **24**,

2039–2055.

6. Santos, J.L.T. & Choi, K.K. Sizing design sensitivity analysis of nonlinear structural systems, part II: numerical method. *Int. J. Num. Meth. in Eng.*, 1988, **26**, 2097–2114.
7. Vidal, C.A., Lee, H.S., & Haber, R.B. The consistent tangent operator for design sensitivity of history-dependent response. *Comp. Syst. in Engng.*, 1991, **2**, 509–523.
8. Vidal, C.A. & Haber, R.B. Design sensitivity analysis for rate-independent elastoplasticity. *Comp. Meth. in Appl. Mech. & Engng.*, 1993, **107**, 393–431.
9. Kleiber, M. Computational coupled non-associative thermoplasticity. *Comp. Meth. in Appl. Mech. & Engng.*, 1991, **90**, 943–967.
10. Kleiber, M., Hien, T.D., & Postek, E. Incremental finite-element sensitivity analysis for non-linear mechanics applications. *Int. J. Num. Meth. in Eng.*, 1994, **37**, 3291–3308.
11. Kleiber, M., Hien, T.D., Antúnez, H., & Kowalczyk, P. Parameter sensitivity of elastoplastic response. *Eng. Comput.*, 1995, **12**, 263–280.
12. Michaleris, P., Tortorelli, D.A., & Vidal, C.A. Tangent operators and design sensitivity formulations for transient non-linear coupled problems with applications to elastoplasticity. *Int. J. Num. Meth. in Eng.*, 1994, **37**, 2471–2499.
13. Badrinarayanan, S. & Zabaras, N. A sensitivity analysis for the optimal design of metal forming processes. *Comp. Meth. in Appl. Mech. & Engng.*, 1996, **129**, 319–348.
14. Simo, J.C. & Taylor, R.L. Consistent tangent operators for rate-independent elastoplasticity. *Comp. Meth. in Appl. Mech. & Engng.*, 1985, **48**, 101–118.
15. Zhang, Q., Mukherjee, S., & Chandra, A. Design sensitivity coefficients for elastoviscoplastic problems by boundary element methods. *Int. J. Num. Meth. in Eng.*, 1992, **34**, 947–966.
16. Zhang, Q., Mukherjee, S., & Chandra, A. Shape design sensitivity analysis for geometrically and materially nonlinear problems by the boundary element method. *Int. J. Solids Struct.*, 1992, **29**, 2503–2525.
17. Leu, L.J. & Mukherjee, S. Sensitivity analysis and shape optimization in nonlinear solid mechanics. *Engng. Anal. with Bound. Elem.*, 1993, **12**, 251–260.
18. Chandra, A. & Mukherjee, S. *Boundary element methods in manufacturing.* Oxford University Press, Oxford, UK., 1997.
19. Wei, X., Leu, L.J., Chandra, A., & Mukherjee, S. Shape optimization in elasticity and elastoplasticity. *Int. J. Solids Struct.*, 1994, **31**, 533–550.
20. Banerjee, P.K. *The boundary element method in engineering (2nd. edition).* McGraw Hill, London, 1994.

21. Jin, H., Runesson, K., & Matiasson, K. Boundary element formulation in finite deformation plasticity using implicit integration. *Comp. & Struct.*, 1989, **31**, 25–34.
22. Telles, J.C.F. & Carrer, J.A.M. Implicit procedures for the solution of elastoplastic problems by the boundary element method. *Mathl. Comput. Modelling.*, 1991, **15**, 303–311.
23. Telles, J.C.F. & Carrer, J.A.M. Static and transient dynamic nonlinear stress analysis by the boundary element method with implicit techniques. *Engng. Anal. with Bound. Elem.*, 1994, **14**, 65–74.
24. Leu, L.J. & Mukherjee, S. Implicit objective integration for sensitivity analysis in nonlinear solid mechanics. *Int. J. Num. Meth. in Eng.*, 1994, **37**, 3843–3868.
25. Leu, L.J. & Mukherjee, S. Sensitivity analysis of hyperelastic-viscoplastic solids undergoing large deformations. *Comp. Mech.*, 1994, **15**, 101–116.
26. Leu, L.J. & Mukherjee, S. Sensitivity analysis in nonlinear solid mechanics by the boundary element method with an implicit scheme. *J. Engng. Anal. & Design*, 1995, **2**, 33–55.
27. Lee, T. H. & Arora, J.S. A computational method for design sensitivity analysis of elastoplastic structures. *Comp. Meth. in Appl. Mech. & Engng.*, 1995, **122**, 27–50.
28. Sladek, J. & Sladek, V. Computation of stresses by BEM in 2D elastostatics. *Acta Technica CSAV*, 1986, **31**, 523–531.
29. Guiggiani, M. Hypersingular formulation for boundary stress evaluation. *Engng. Anal. with Bound. Elem.*, 1994, **13**, 169–179.
30. Hodge, P.G. & White, G.N. A quantitative comparison of flow and deformation theories of plasticity. *J. Appl. Mech.*, 1950, **17**, 180–184.
31. Arif, A.F.M. & Zabaras, N. On the performance of two tangent operators for finite element analysis of large deformation inelastic problems. *Int. J. Num. Meth. in Eng.*, 1992, **35**, 369–389.

APPENDIX

Here we present an exact solution for the hollow cylinder subjected to equal internal and external pressures of 0.01 (example 3).

Using the kinematic fact that the radial strain equals the hoop strain, and exploiting the in-plane symmetry of the situation, the final stress can be written as:

$$\boldsymbol{\sigma} = \begin{bmatrix} \sigma_{rr} & & \\ & \sigma_{\theta\theta} & \\ & & \sigma_{zz} \end{bmatrix} = \begin{bmatrix} -0.01 & & \\ & -0.01 & \\ & & a \end{bmatrix}$$

where $a < 0$ is our first unknown. The mean normal stress is

$$\sigma_m = \frac{a - 0.02}{3}$$

and the deviatoric stress,

$$\boldsymbol{\sigma}' = \begin{bmatrix} \frac{-0.01-a}{3} & & \\ & \frac{-0.01-a}{3} & \\ & & \frac{2a+0.02}{3} \end{bmatrix}$$

The von Mises equivalent stress is

$$\kappa = \sqrt{\frac{3}{2}\boldsymbol{\sigma}' : \boldsymbol{\sigma}'} = 0.01 + a$$

so the consistency condition reads:

$$0.01 + a = 2G(0.001 + k_1 \bar{e}^p) \tag{A.1}$$

where the equivalent plastic strain, $\bar{e}^p$, is our second unknown.

Meanwhile, the strain is given by:

$$\boldsymbol{\varepsilon} = \begin{bmatrix} b & & \\ & b & \\ & & 0 \end{bmatrix}$$

where $b < 0$ serves as our third unknown.

Recalling that the plastic strain shares the same direction as the deviatoric stress, we write:

$$\boldsymbol{\varepsilon}^p = \bar{e}^p \begin{bmatrix} -\frac{1}{2} & & \\ & -\frac{1}{2} & \\ & & 1 \end{bmatrix}$$

where the matrix components have been scaled to conform to the definition:

$$\bar{e}^p = \sqrt{\frac{2}{3}\boldsymbol{\varepsilon}^p : \boldsymbol{\varepsilon}^p}$$

The elastic strain is

$$\boldsymbol{\varepsilon}^e = \boldsymbol{\varepsilon} - \boldsymbol{\varepsilon}^p = \begin{bmatrix} b + \frac{\bar{e}^p}{2} & & \\ & b + \frac{\bar{e}^p}{2} & \\ & & -\bar{e}^p \end{bmatrix}$$

with a deviatoric part

$$\boldsymbol{\varepsilon}^{e\prime} = \begin{bmatrix} \frac{b}{3} + \frac{\bar{e}^p}{2} & & \\ & \frac{b}{3} + \frac{\bar{e}^p}{2} & \\ & & -\bar{e}^p - \frac{2b}{3} \end{bmatrix}$$

The dilatational part of Hooke's law reads:

$$\sigma_m = K(\epsilon_{11} + \epsilon_{22} + \epsilon_{33})$$

$$\frac{a - 0.02}{3} = \frac{2G(1+\nu)}{3(1-2\nu)} 2b \qquad (A.2)$$

where the bulk modulus K has been expressed in terms of the shear modulus G and Poisson's ratio ν. Finally, the deviatoric part of Hooke's law is

$$\boldsymbol{\sigma}' = 2G\boldsymbol{\varepsilon}^{e\prime}$$

$$\frac{-0.01 - a}{3} = 2G(\frac{b}{3} + \frac{\bar{e}^p}{2}) \qquad (A.3)$$

(A.1), (A.2), and (A.3) form a linear system of equations for the unknowns a, b, and $\bar{e}^p$. The solution for $\bar{e}^p$ is (upon substituting in the given values for G and ν)

$$\bar{e}^p = \frac{-0.03}{-39 - 30k_1}$$

The sensitivity w.r.t. k_1 follows upon differentiation

$$\begin{aligned} \frac{d}{dk_1}\bar{e}^p &= \frac{-0.9}{(-39 - 30k_1)^2} \\ &= -5.9080669 \times 10^{-4} \qquad \text{at } k_1 = 0.001 \end{aligned}$$

	without averaging		with averaging	
r	value	% error	value	% error
1.000	-5.8908e-04	0.292	-5.9070e-04	0.0169
1.125	-5.8882e-04	0.336	-5.9019e-04	0.104
1.250	-5.9154e-04	0.124	-5.9054e-04	0.0445
1.375	-5.8927e-04	0.260	-5.9029e-04	0.0860
1.500	-5.9176e-04	0.161	-5.9058e-04	0.0369
1.625	-5.8921e-04	0.270	-5.9037e-04	0.0736
1.750	-5.9069e-04	0.0197	-5.9048e-04	0.0552
1.875	-5.8988e-04	0.156	-5.9055e-04	0.0420
2.000	-5.8902e-04	0.302	-5.9075e-04	0.00834

Table 1. Sensitivity of equivalent plastic strain w.r.t. k_1
BEM results – example 3

List of titles of Figures and Tables

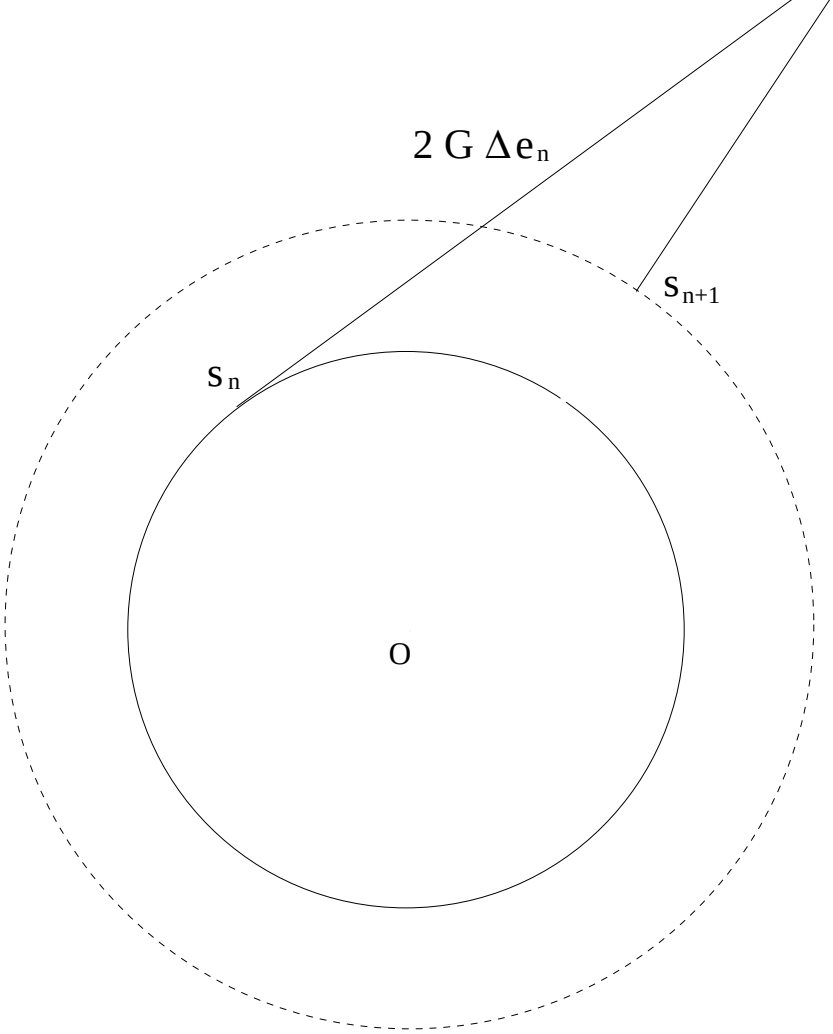

Figure 1. Illustration of the RRA

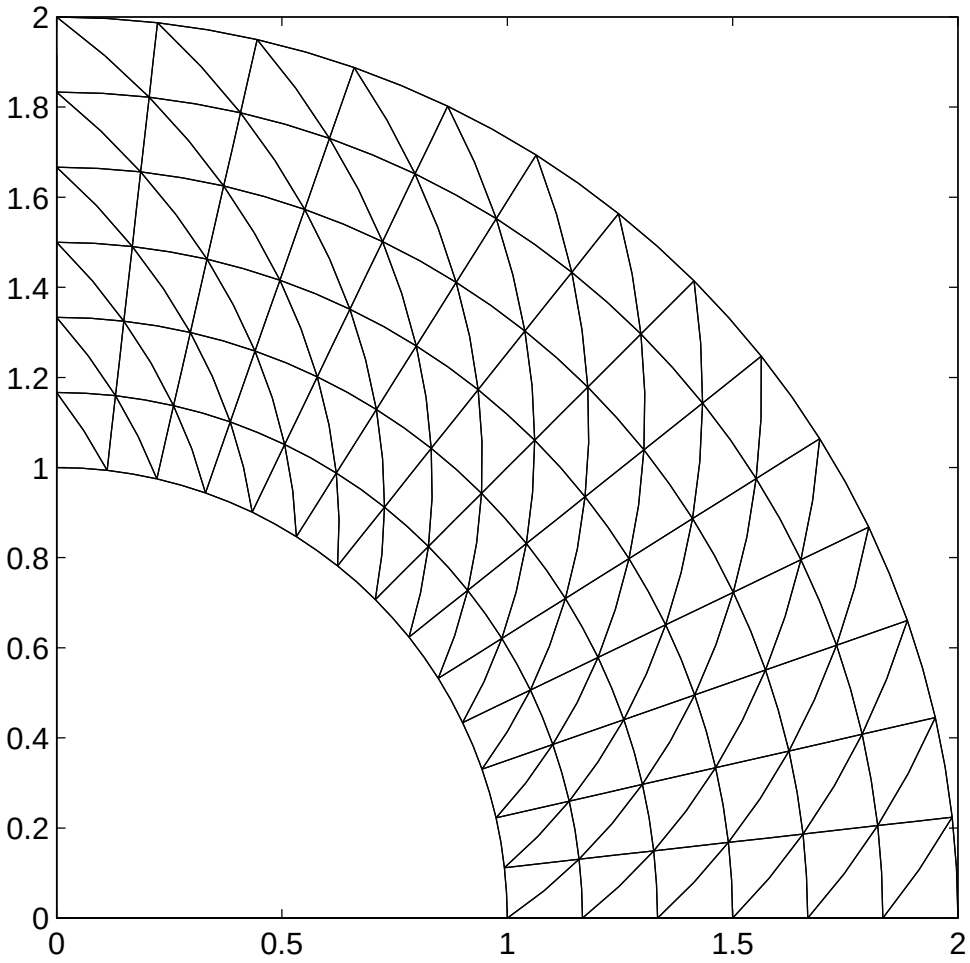

Figure 2. BEM mesh

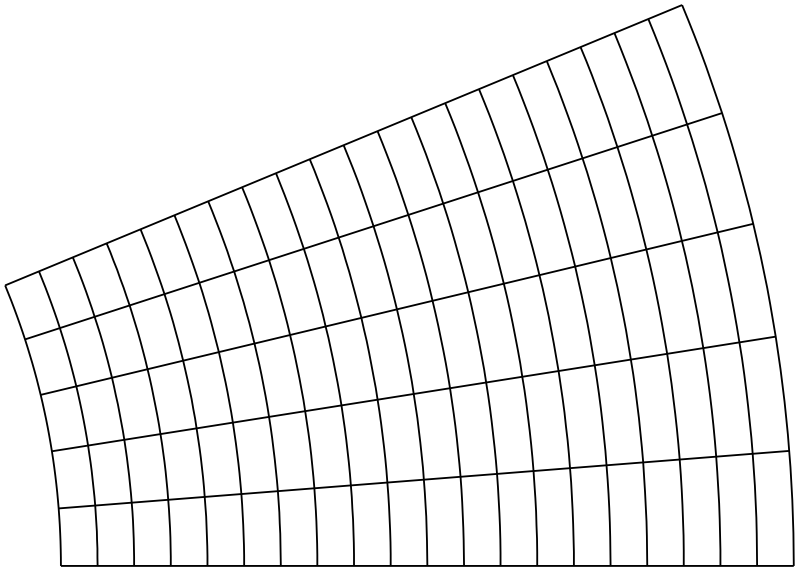

Figure 3. FEM mesh

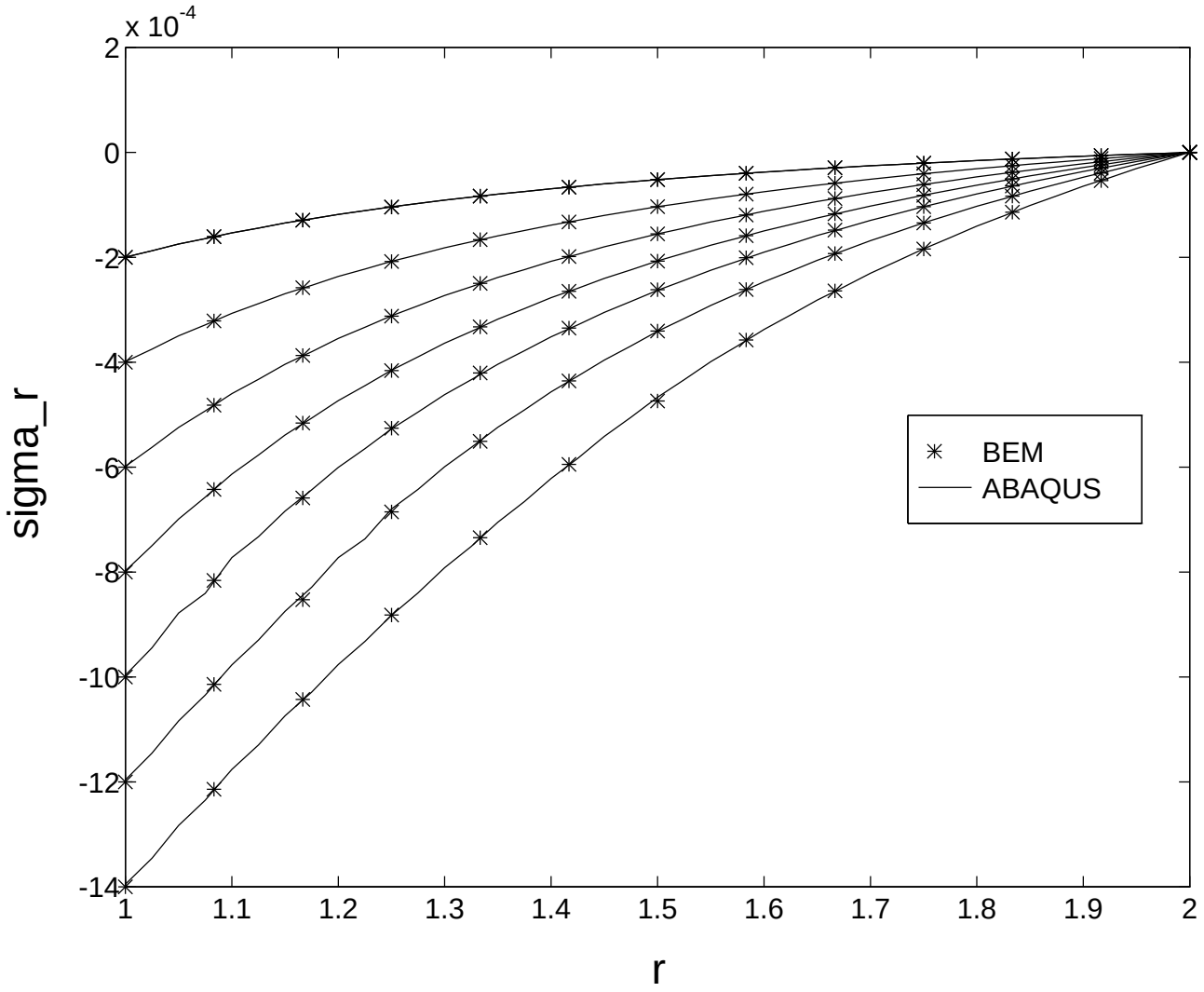

Figure 4. Radial stress – linear hardening
Comparison of BEM and FEM results (example 1)

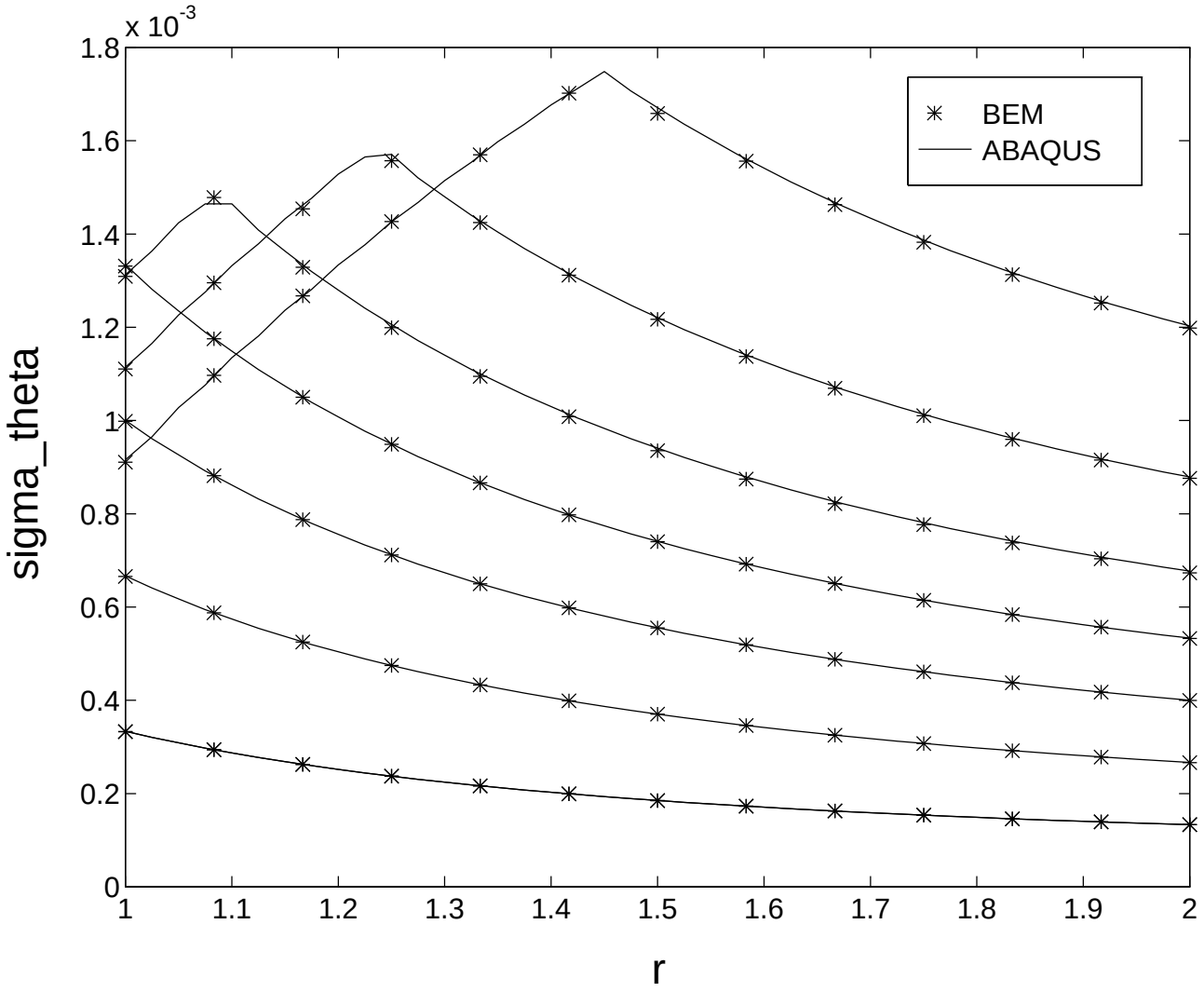

Figure 5. Hoop stress – linear hardening
Comparison of BEM and FEM results (example 1)

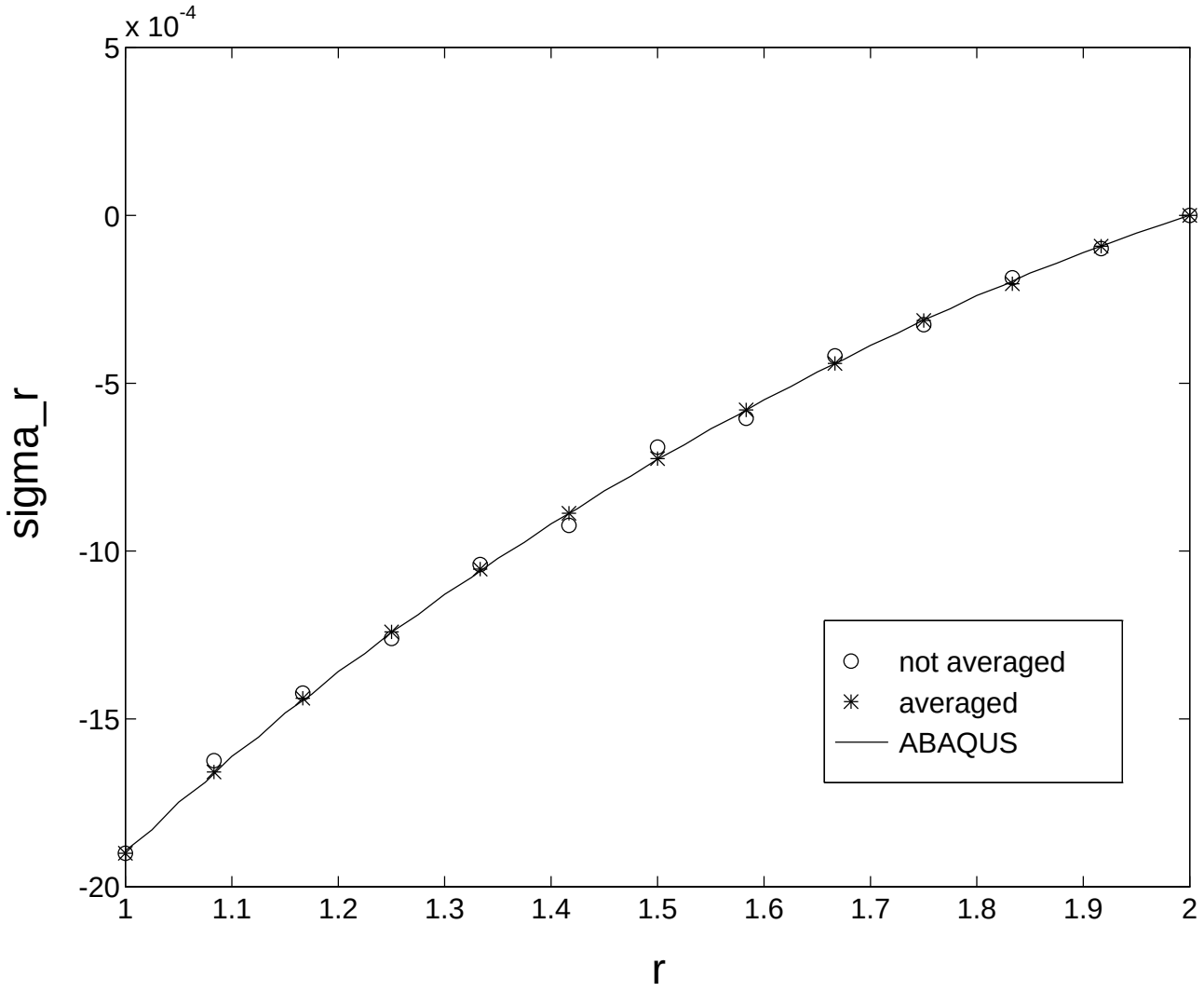

Figure 6. Radial stress – nonlinear hardening
Comparison of BEM and FEM results (example 2)

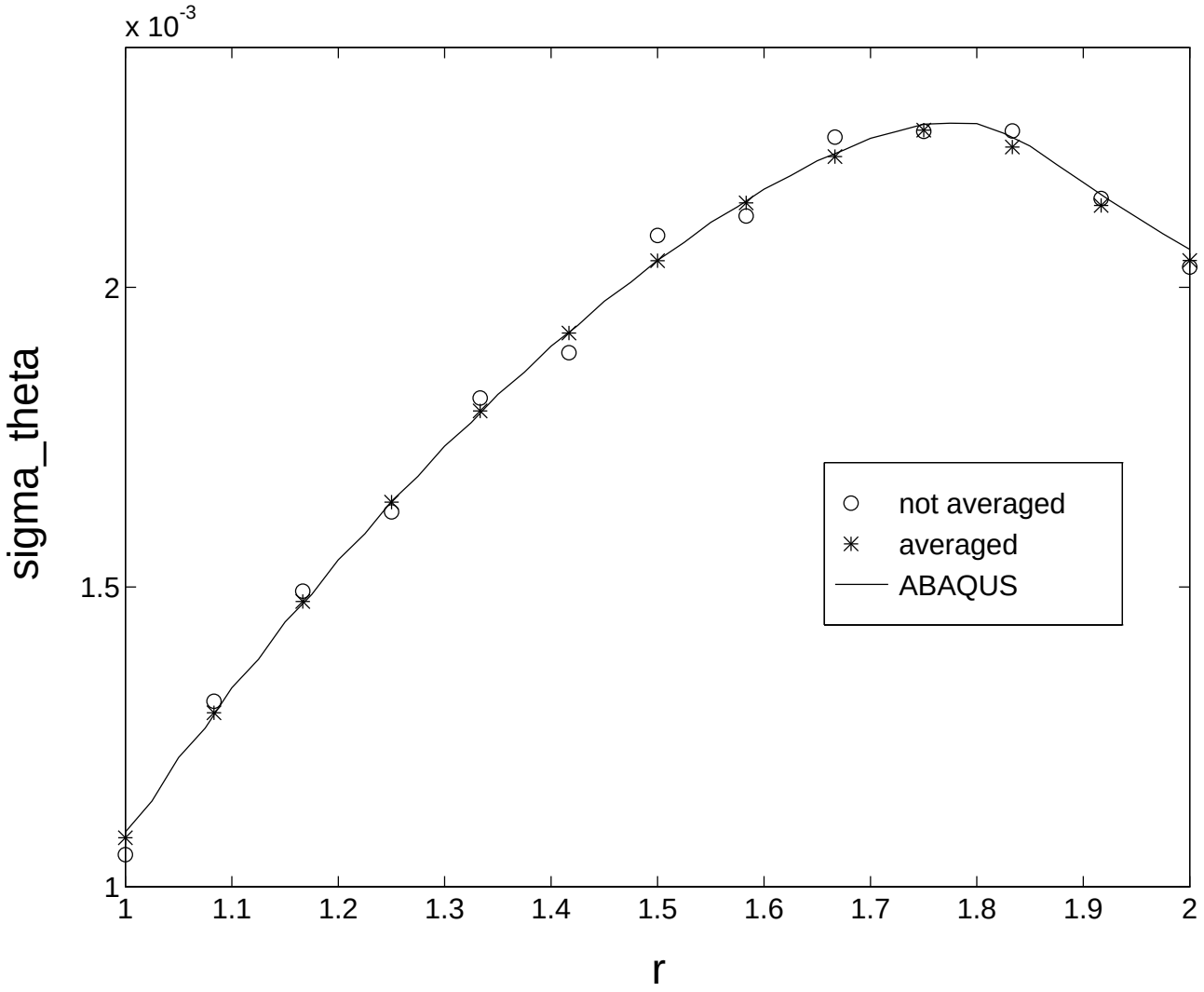

Figure 7. Hoop stress – nonlinear hardening
Comparison of BEM and FEM results (example 2)

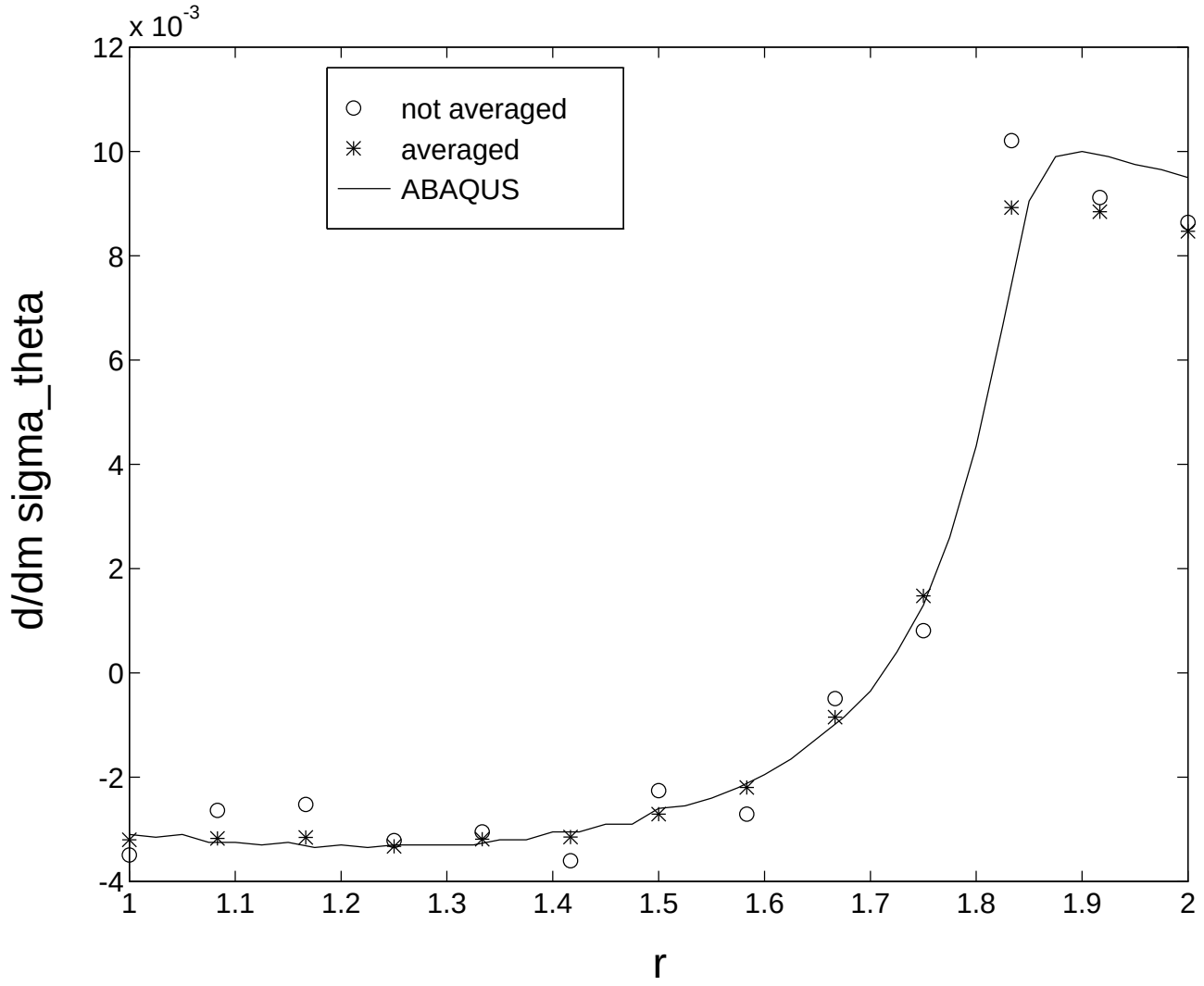

Figure 8. Sensitivity of hoop stress w.r.t. m – nonlinear hardening
Comparison of BEM and FEM results (example 2)

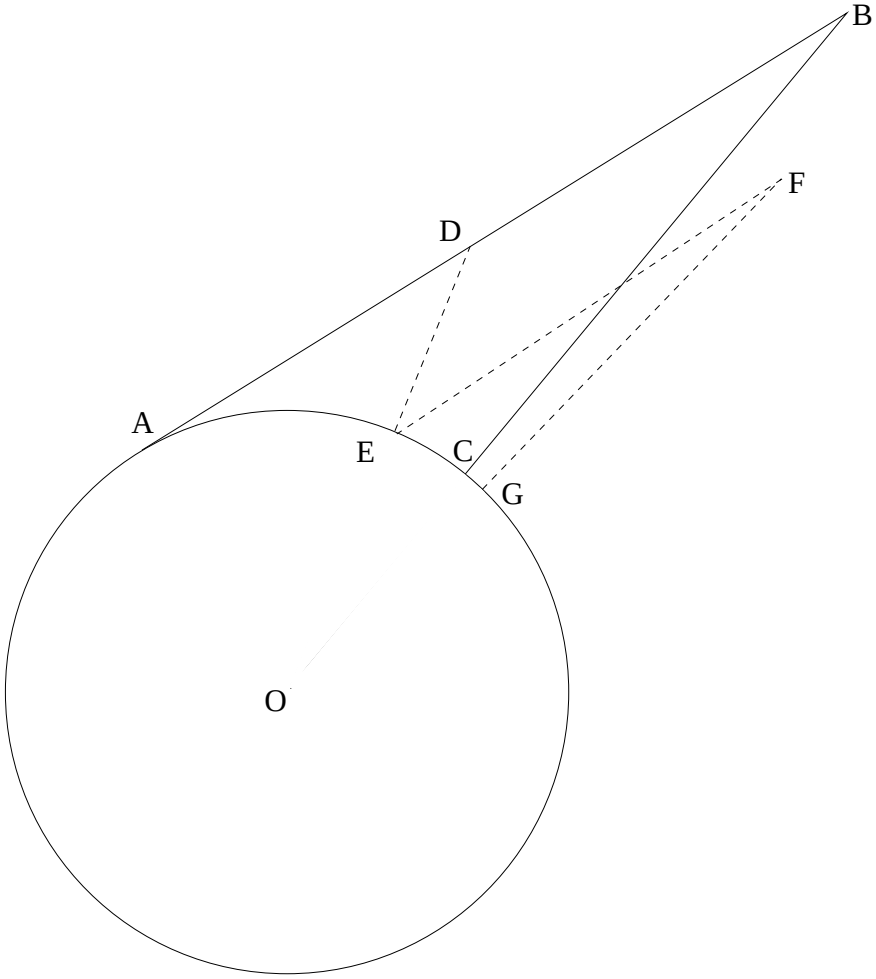

Figure 9. Basic mechanism by which the RRA outcome depends on load step size